# Numerical simulations of TiO 2 production in a laminar coflow H 2 /Ar/TTIP diffusion flame: Comparison with experiments and parametric sensitivity study

B. Franzelli, J. Bonnety, J. Yi, Y. Ogata, A. Cuoci, C. Betrancourt

# Numerical simulations of $TiO_2$ production in a laminar coflow $H_2$/Ar/TTIP diffusion flame: comparison with experiments and parametric sensitivity study

B. Franzelli[a,*], J. Bonnety[a], J. Yi[a], Y. Ogata[a], A. Cuoci[b], C. Betrancourt[a]

[a] *EM2C laboratory, CNRS, CentraleSupelec, 3 rue Joliot Curie, 91192 Gif-sur-Yvette, France*
[b] *CRECK Modeling Lab, Department of Chemistry, Materials, and Chemical Engineering, Politecnico di Milano, P.zza Leonardo da Vinci 32, Milano, Italy*
∗ *Corresponding author: benedetta.franzelli@centralesupelec.fr*

**Abstract**

Metal-oxide nanoparticles are paving the way for the development of new materials, and flame spray pyrolysis (FSP) systems are gaining attention for their large-scale production. On an industrial level, precise control of particle characteristics is needed while guaranteeing an almost zero-emission process. In this context, computational fluid dynamic (CFD) simulations of nanoparticle production in flames are sought to optimize the design of FSP systems. In this work, numerical simulations of $TiO_2$ nanoparticles production from Titanium(IV) isopropoxide (TTIP) are performed for a laminar coflow $H_2$/Ar flame as a first step towards this objective. To lower the CPU cost for 2-D simulations, reduced descriptions for the gas phase and for nanoparticles are considered. For $H_2$ combustion, a 10-species kinetic mechanism is retained. Five different submechanisms are tested for the description of TTIP conversion into $Ti(OH)_4$, considered as the $TiO_2$ precursor. The description of the solid phase relies on a classical three-equation monodisperse formulation. The objective of this work is not to validate the considered CFD strategy, for which a more extensive database would be required, but to identify the most relevant processes for flame synthesis in a diffusion flame by performing a parametric sensitivity study. The originality of this investigation relies on the study of particle characteristics along an $H_2$ laminar flame in a non-premixed configuration. Thus, the focus of the parametric study is on the effect on nanoparticle characteristics of: 1) diffusion processes of gaseous phase and nanoparticles; 2) aerosol processes. Numerical results are compared to experimental data in terms of conversion rate, volume fraction, and primary particle diameter along the flame height. Trends from the literature on the effect of aerosol process parameters are retrieved. Results highlight the key role of diffusion processes on nanoparticle production in non-premixed flames and the need for future improvements of TTIP conversion kinetics.

*Keywords:* $TiO_2$ flame synthesis; nanoparticle numerical simulations; parametric sensitivity study; laminar coflow diffusion flame; SEM; LII

## 1. Introduction

Nanoparticle synthesis via flame spray pyrolysis (FSP) systems is a promising alternative for the large-scale production of metal-oxides, such as titanium dioxide ($TiO_2$), with tailored characteristics [1, 2]. For this, precise control of turbulent spray combustion is needed since the particle characteristics such as size and morphology, which greatly govern the performances of the final material, are the result of local ambient conditions that they experience during the aerosol processes [3]: nucleation; condensation and surface growth; coagulation and aggregation; sintering. In this context, disposing of computational fluid dynamics (CFD) simulations, which provide complementary information to experiments, would be of great value as an essential tool for the rational design of nanoparticles. However, before addressing the numerical challenges in realistic configurations, it is essential to evaluate the performances of the retained numerical strategies on academic flame configurations that reproduce the main aerosol processes under simplified conditions, i.e. laminar steady conditions and pre-vaporization of liquid metal-alkoxides.

Concerning $TiO_2$ production in laminar flames from pre-vaporized TTIP (titanium(IV) isopropoxide), which is the focus of the present investigation, various experimental databases can be found in the literature. Nanoparticles production in premixed flames has been characterized considering $CH_4$, $C_2H_4$ and $H_2$ as fuels [4–8]. Premixed configurations present some major advantages compared to non-premixed flames. By imposing the mixture equivalence ratio, it is possible to control the temperature and, more generally, the local gaseous conditions experienced by the particles along their trajectory. The effect of the operating conditions on particle characteristics can then be studied in a straightforward manner. In addition, premixed configurations are usually assumed as one-dimensional[1], so that their experimental study is easier compared to 2-D configurations. For the same reason, their simulation requires small CPU resources. For all these reasons, laminar pre-vaporized premixed flames represent the ideal configurations for the validation of detailed models for the gaseous phase, such as kinetic schemes for TTIP decomposition and hydrolysis, [10, 11] and for the nanoparticles, considering that sophisticated models, such as moving sectional methods [12] or statistical approaches [13], can be applied by postprocessing the gaseous fields as a function of the particle residence time. Therefore, the sensitivity of the model's parameters has already been extensively analyzed using detailed descriptions of both gas and solid phases in premixed flame configurations [14].

Complementary to premixed flames, $TiO_2$ production in non-premixed configurations can also be considered. Contrary to premixed-flames, any change of the operating conditions in a diffusion flame will affect nanoparticle production in both direct and indirect ways since the local mixture fraction field and, consequently, the whole gaseous phase will be modified due to the intrinsic nature of diffusion flames. However, their study is of great interest since non-premixed configurations are expected to be more representative of aerosol processes in FSP systems. Synthesis in non-premixed flames has been studied in the literature mainly in methane/oxygen coflow diffusion-flames [15–17], considering the effect of reactant mixing, flow rates, and configurations on nanoparticle characteristics. Memon et al. [18] considered the effect of fuel composition ($H_2$ and $C_2H_4$) in multiple-diffusion flames on the growth of pure anatase and carbon-coated titanium dioxide. Ren et al [19] considered $C_2H_4$ counterflow flames to investigate the effect of flow rate on the size and morphology of carbon nanocomposites. Recently, Yi et al [20] investigated $TiO_2$ production in an $H_2$/Ar/TTIP flame by performing 2-D laser-induced incandescence (LII) measurements of $TiO_2$ volume fraction $f_v$ in the whole flame. This configuration is of interest for many reasons:

- It is an unconventional combustion application of future *'green'* $H_2$. Even if flame synthesis of metal-oxides represents a promising alternative to produce nanopowder, it must be guaranteed that this aereosol technology does not contribute to negative emissions. The use of $H_2$ is a valuable starting point in this direction since: 1) $H_2$ has the potential to produce nanoparticles in a cleaner way compared to carbon-based fuels; 2) $H_2$ itself can be potentially produced in a â€˜greenâ€™ way; 3) $TiO_2$ is one of the most promising photocatalysists for $H_2$ production itself.
- The $H_2$ combustion presents simple kinetics, simplifying the model validation task.
- The geometry of the configuration reproduces the YDB (Yale Diffusion Burner) burner, which is extensively used for the study of soot production in the framework of the International Workshop on the measurement and computation of reacting flows with carbon nanoparticles (ISF workshop). Experimental and numerical tools for the study of the combustion processes in this configuration are then well-established in the literature [21–23].
- Information on the spatial evolution of $f_v$ in the combustion zone can be considered to study the early formation of particles and to evaluate the performances of different submodels for the description of this stage.
- It allows the study of nanoparticle production and the validation of the CFD strategy in a configuration where diffusion processes are expected to be more relevant than in premixed configurations.

For all these reasons, this configuration is considered in this work to perform numerical simulations of $TiO_2$

[1] The validity of such assumption has been studied in [9].

production in an $H_2$/Ar/TTIP coflow diffusion flame. The objective of this work is not to validate the considered models for which a more extensive experimental database would be necessary, but to evaluate the sensitivity of the model's parameters in non-premixed configurations. This will allow us to complete the sensitivity analysis already available for premixed cases [14] and to identify the most relevant processes in non-premixed flame synthesis, whose modeling should be the focus of future works. For this, the performances of different submodels will be evaluated by comparing the numerical results with: 1) already published experimental 2-D field of volume fraction [20]; 2) new experimental data on mean primary particle size $d_p$ obtained via scanning electron microscope (SEM) at different flame heights. The paper is organized as follows. First, the experimental setup is described in Sec. 2 for both LII and SEM measurements to obtain information on conversion rate, $TiO_2$ volume fraction and mean primary particle diameter $d_p$. Second, the numerical strategy retained in this work is summarized in Sec. 3. Models considered here are less sophisticated than state-of-the-art approaches for 1-D premixed simulations [13]. This is needed to perform a parametric study of 2-D configurations for an affordable CPU cost. It also allows the evaluation of the performances of simplified descriptions that have the potential to be used in the future for 3-D simulations of realistic configurations. Finally, results for volume fraction and primary particle diameter $d_p$ are compared to the experimental database in Sec. 4. The sensitivity study is performed by considering the effect of individual parameters: 1) five different schemes for TTIP conversion; 2) diffusive processes of gaseous Ti-containing species and of nanoparticles; 3) aerosol process parameters.

## 2. Experimental configuration

The considered configuration corresponds to the Yale diffusion burner (YDB) [21–23]. It consists of a stainless-steel inner tube for fuel/inert gas injection with a diameter of $D_{in}$=3.9 mm and a wall thickness of 0.5 mm. It is surrounded by a concentric air coflow of a diameter of 76 mm. The air passes through 3 mm glass beads and two layers of honeycomb sections (cell size of 0.8 mm) to obtain uniform straightened flow without flow disturbances. A thermalized version of the YDB burner with a pre-vaporized injection system has been developed so that TTIP is fully evaporated in the fuel mixture before reaching the exit of the injection tube [20]. The typical luminosity of $H_2$ flame with TTIP injection is presented in Fig. 1a. A light blue zone, localizing the combustion zone, is observed at z<25 mm. The strong luminous cylindrical zone indicates the presence of $TiO_2$ nanoparticles. The operating conditions considered in this work are the same of [20]: mass flow rate 5.1 g/h for $H_2$, 2.3 g/h for Ar, 0.5 g/h for TTIP. Temperatures at injection are measured with thermocouples (K-type): 380K in the inner flow, 412 K in the coflow. Hot air coflow was maintained at 5.5 m/s.

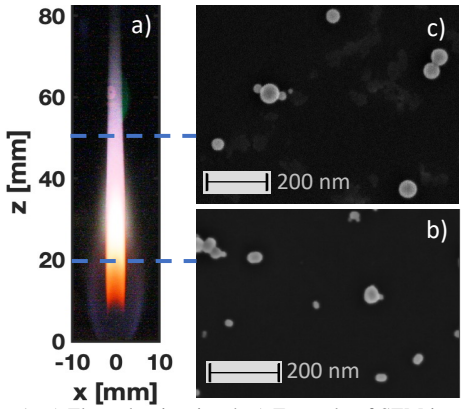

Fig. 1: a) Flame luminosity. b-c) Example of SEM images at b) HAB=20 mm and c) HAB=50 mm.

### 2.1. Experimental setup for LII

The LII experimental setup is the same described in [20] and is briefly reminded in this section. A 10Hz Nd:YAG laser beam (Quantel, Q-smart 850) at 355 nm is shaped into a nearly top-hat: 8 mm in $x$ direction, 1 mm in $z$ direction and 1 mm in $y$ direction. An intensified camera (Princeton Instruments, PI-MAX 4, 1024i) equipped with a filter centered at 640 nm Â± 7 nm (Edmund optics, 86995) was used to obtain the spatial distribution of LII signal using a fluence of 0.15 J/cm2 to prevent any interferences [24]. LII measurements are performed at different flame heights every 2 mm, by moving the burner in the z-direction with an accuracy of 0.01 mm. It is important to remind that the use of the LII technique to obtain information on $f_v$ of $TiO_2$ on this flame has been extensively validated in [20]. In specific, at the considered fluence 1) no fluorescence of TTIP has been observed; 2) the LIE signal has a LII-like behavior; 3) the LII signal can be interpreted as directly proportional to $f_v$. The LII measurement showed a 30% of standard deviation variation most likely because $TiO_2$ production is not perfectly steady in the flame indicating the need for future improvements of the injection systems.

### 2.2. Experimental setup for SEM

The SEM samples are collected thermophoretically [25] by insertion of a square silicon wafer (10x10 $mm^2$ Micro to Nano 10-008149) into the flame. The sampling system is described in details in Betrancourt et al. [26]. A brief overview is given here. A silicon wafer is installed on a support connected to a stepper motor allowing a repetitive swing movement across a horizontal plane parallel to the burner surface. The spatial resolution along the flame $z$-axis is estimated to +/- 0.5 mm. The mean insertion velocity is 0.19 m/s. The wafer crosses the entire flame orthogonally to the flame $z$-axis. It has to be reminded that inserting the wafer can modify the particles properties as any other sampling process. To min-

imize its effect and specifically to reduce the possible superposition of various particles, only one swing of the wafer is considered and its residence time in the flame is optimized, here approximately 30 ms, to have enough particles while limiting particle overcrowding, i.e. artificial primary particles aggregation. As a result, the primary particle size $d_p$ is expected to be only slightly affected during the sampling procedure and this is the only information that is extracted from SEM images in this work. To exploit SEM images to obtain additionally information, such as the number of primary particles per aggregate, a systematic study should be performed by considering different wafer velocities and numbers of swing, which is out of the scope of this article.

The particles are collected at $z$=20, 30, 45, 60 and 80 mm. Due to the lateral swing movement, particles are preferentially collected on the edges of the flame, characterized by a longer residence time. However, the thermophoretically sampling is expected to be more efficient at the flame centerline, where the maximum particles volume fraction is localized (see Fig. 3).

The samples are analyzed by a Scanning electron microscope (SEM Leo 1530 Gemini, Carl Zeiss) The images are recorded at a beam energy of 1.9 keV. The SEM images were processed using the free software ImageJ. The individual primary particles are considered spherical and their size is measured for isolated particles and for primary particles in aggregates. Typical images are displayed in Figs. 1b and c for z=20 and 50 mm, respectively. Additional images are provided in the Supplementary Materials together with the histograms for primary particle diameter $d_p$. Experimental diameter values reported in the following correspond to the arithmetic mean.

## 3. Numerical setup

The laminarSMOKE++ solver [27], developed at Polimi, has been extended to describe $TiO_2$ nanoparticles. The YDB burner is simulated by assuming axis-symmetry. The numerical mesh represents an axial 2D-plane, which extends over $0 < x < 3.8$ cm and $-0.25 < z < 12$ cm. The grid accounts for 14000 cells with a spatial resolution in the reaction zone of approximately 0.18 mm. Boundary conditions are provided in Table 1. To simulate $TiO_2$ production in $H_2$/Ar/TTIP flames, three submodels are needed:

1. A kinetic mechanism for fuel combustion. In this work, hydrogen combustion is described by a 10-species and 23-reactions model developed by Polimi [28].
2. A kinetic mechanism for the description of TTIP conversion into $Ti(OH)_4$ considered here as the gaseous precursor. Details on the mechanisms retained in this work are provided in Sec. 3.1.
3. The solid phase formation and evolution models described in Sec. 3.2.

| Inflow | | | | | Coflow | |
|---|---|---|---|---|---|---|
| $Y_{H_2}^{in}$ [−] | $Y_{A_r}^{in}$ [−] | $Y_{TTIP}^{in}$ [−] | $u^{in}$ [m/s] | $T^{in}$ [K] | $u^{co}$ [m/s] | $T^{co}$ [K] |
| 0.646 | 0.291 | 0.063 | 1.902 | 380 | 0.556 | 412 |

Table 1: Numerical boundary conditions.

### *3.1. Kinetic models for TTIP conversion*

Concerning the conversion of TTIP into titanium (IV) hydroxide ($Ti(OH)_4$), different families of kinetic descriptions with increasing complexity and CPU cost can be found in the literature (global, reduced, detailed schemes). In this work, five mechanisms, whose CPU cost is affordable for 2-D and 3-D simulations, are considered:

- Model 1. A global scheme describing the TTIP thermal decomposition as: TTIP $\rightarrow$ $H_4O_4Ti + 4C_3H_6$ The reaction rate follows an Arrhenius law, whose reaction rates are given by [29].
- Model 2. A one-step reaction is added to model 1 to account for TTIP hydrolysis: TTIP + $2H_2O \rightarrow H_4O_4Ti + 3C_3H_6 + 3CH_3 + HO_2$ The reaction parameters come from [30].
- Model 3. A reduced mechanism, composed of 25 Ti species and 61 reactions, is considered to describe the thermal decomposition of TTIP, occurring via $C_3H_6$ abstraction and $CH_3$/H abstractions [13].
- Model 4. To account for hydrolysis for a small CPU cost, four representative hydrolysis reactions, listed in Table 2, have been added to model 3. Parameters for reaction R1 come from [31]. Reaction parameters for R2-R4 have been obtained in analogy with the kinetics of Buerger et al. [11], based on [32].
- Model 5. The thermal decomposition ($C_3H_{10}O_4 \rightarrow Ti(OH)_4 + C_3H_6$) and hydrolysis (R4 of Table 2) pathways for $C_3H_{10}O_4$ are deleted from model 3 so that no direct conversion of $C_3H_{10}O_4Ti$ into $Ti(OH)_4$ can occur. With this model, $Ti(OH)_4$ originates only from chemical pathways involving $Ti(OH)_3$ or $H_3O_4Ti$.

To guarantee mass and enthalpy conservation, a dummy gaseous species ($TiO_2Ru$) is added to all five models to reproduce the conversion of $Ti(OH)_4$ into $TiO_2$ [33]. The effect of the five models on the prediction of $TiO_2$ production will be analyzed at Sec. 4. For all mechanisms, thermodynamic and transport properties for gaseous Ti-containing species come from [11], where they were derived in analogy from [32]. Soret effect is included in all simulations.

### *3.2. Solid phase description*

As for the gaseous phase, various models with different levels of accuracy and cost can be found in the literature for nanoparticle production in flames.

| Reaction | $A$ [cm$^3$.mol$^{-1}$.s$^{-1}$] | $\beta$ | E [cal/mol] | Ref. |
|---|---|---|---|---|
| R1) $C_{12}H_{28}O_4Ti + H_2O \rightarrow C_9H_{22}O_4Ti + IC_3H_7OH$ | $1.23 \cdot 10^{14}$ | 0 | 22 501 | [31] |
| R2) $C_9H_{22}O_4Ti + H_2O \rightarrow C_6H_{16}O_4Ti + IC_3H_7OH$ | $9.22 \cdot 10^{13}$ | 0 | 22 501 | [32] (analogy) |
| R3) $C_6H_{16}O_4Ti + H_2O \rightarrow C_3H_{10}O_4Ti + IC_3H_7OH$ | $6.15 \cdot 10^{13}$ | 0 | 22 501 | [32] (analogy) |
| R4) $C_3H_{10}O_4Ti + H_2O \rightarrow H_4O_4Ti + IC_3H_7OH$ | $3.08 \cdot 10^{13}$ | 0 | 22 501 | [32] (analogy) |

Table 2: Four-step submechanism for TTIP hydrolysis for models 4 and 5. Reaction R4 is not considered in model 5. $A$, $\beta$ and $E$ are the pre-exponential constant, the temperature dependency and the activation energy, respectively, of an Arrhenius law.

Among them, monodisperse models provide a reasonable estimation of the aerosol process for a small CPU cost to perform extensive parametric studies on 2-D and 3-D configurations and/or numerical simulations of turbulent realistic burners. In this work, a three-equation model originally developed for soot [34] is adapted to the description of $TiO_2$ formation. Three-equation models are often used for the simulation of metal-oxides flame synthesis (cfr. for example, [35–37]). The main difference with the model considered in this work is that it accounts for condensation, as done for example in [14], to investigate the contribution of this process to metal-oxides production in comparison with nucleation, sintering and coagulation. The retained model is based on the transport of the total number density $N_p$, the total surface $S_p$ and the mass fraction $Y_p = \rho_p \rho^{-1} f_v$ ($\rho$ and $\rho_p$ are the gas and particle density, respectively). The mean particle volume and surface are $v_p = f_v N_p^{-1}$ and $s_p = S_p N_p^{-1}$, respectively. The mean primary particle diameter is $d_p = 6 v_p s_p^{-1}$. Thermophoresis is accounted for $TiO_2$ nanoparticles and the particle diffusivity is $D_p = k_b T/(3\pi\mu d_c)$, where $\mu$ is the gas viscosity. Nucleation, condensation, coagulation and sintering are described by assuming a monodisperse population. Their formulation is explicited in the Supplementary Material. In Section 4.2, the sensitivity of the following model's parameters will be evaluated: nucleation, condensation, and coagulation collisional frequencies ($\epsilon_{nu}$, $\epsilon_{cd}$,$\epsilon_{cg}$, respectively) and the sintering time $\tau_{sint}$. Their reference values and additional model's details are provided in Supplementary Material. The modelâ€™s parameters were chosen among values classically retained in the literature for nanoparticles (soot and metal-oxides) simulations. It is important to reminded that since a parametric study is performed, the general conclusions will not depend on the value initially retained for the reference case.

## 4. Results

The effect of the different submechanisms is evaluated on $TiO_2$ production in a coflow $H_2$/Ar/TTIP diffusion flame. First, the performances of the five kinetic schemes for TTIP conversion are evaluated by considering the same models for the description of fuel combustion and solid phase. It has been verified that the prediction of temperature, velocity and major species, such as $H_2O$ and $H_2O_2$, does not vary between the simulations. At a given height above the burner $z$, the conversion yield $\eta(z)$ of TTIP into $TiO_2$ mass can be defined as the ratio of mass flux of Ti elements from $TiO_2$ at position $z$ over the inlet mass flux of Ti elements from TTIP:

$$\eta(z) = \frac{\int_0^R \rho_p u_z W_{TiO_2}^{-1} f_v r dr}{\rho^{in} u_z^{in} W_{TTIP}^{-1} Y_{TTIP}^{in} D_{in}^2/8} \qquad (1)$$

where $r$ is the radial coordinate, $u_z$ is the axial velocity and 'in' indicates inlet conditions. The evolution $\eta(z)$ for the five mechanisms is illustrated as a function of the flame height $z$ in Fig. 2. Results of $f_v$ along the flame centerline normalized by its value $f_v^0$ at $z$=50 mm are also provided in the bottom. Results with the five kinetic models are compared to experimental LII data. When accounting for hydrolysis, both global and reduced schemes (models 2 and 4, respectively) predict a too-soon and too-quick conversion compared to experiments. Even without hydrolysis, the global scheme (model 1) over-predicts the conversion rate. Overall, models 3 and 5 present a better agreement with the experimental data. By looking at the results on the normalized volume fraction at the bottom of Fig. 2, it can be deduced that by neglecting the direct conversion of $C_3H_{10}O_4Ti$ into $(OH)_4Ti$, the conversion process slows down. Overall, the best agreement with experiments is observed with model 5. Still, the conversion process seems to be too quick. It has been verified that the spatial evolution of the conversion yield is largely governed by the kinetics of TTIP conversion into $(OH)_4Ti$, almost independently from the parameters of the solid phase model. Thus, results of Fig. 2 seem to indicate that improvements in the description of the kinetic mechanism for TTIP conversion into gaseous precursors of $TiO_2$ are needed to more precisely capture the evolution of the conversion yield along the flame height. However, the agreement of the model 5 with the experiments can be considered reasonable enough to perform the sensitivity study on the model's parameter on nanoparticle production in the following by focusing on diffusion and aerosol processes.

### *4.1. Effect of transport properties of gaseous Ti-containing species*

When considering non-premixed configurations, the diffusive processes are expected to play an essential role in nanoparticle production. To investigate this, different numerical simulations were performed

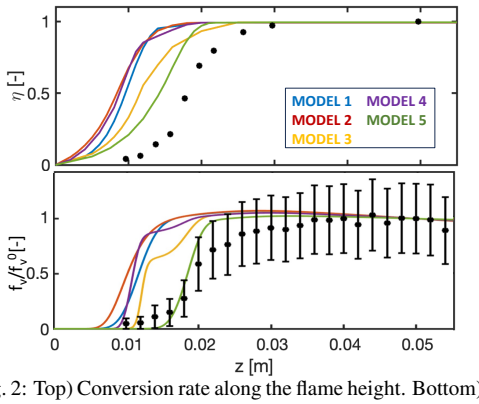

Fig. 2: Top) Conversion rate along the flame height. Bottom) $TiO_2$ volume fraction along the flame centerline normalized by its value $f_v^0$ at $z$=50 mm. Results for five submodels for TTIP conversion are compared to LII results (symbols).

using model 5 and keeping the parameters describing the aerosol processes unchanged.

The diffusion coefficients $D_k^{Ti}$ of Ti-containing gaseous species were reduced by a factor of 2, 4, and 10 to study the role of diffusive processes in nanoparticle production. Results for the 2-D spatial distribution of $f_v$ normalized by the maximum value $f_v^{max}$ obtained for each case are illustrated in Fig. 3 and compared to experimental results. For the reference values of $D_k^{Ti}$, the maximum value of $f_v$ is observed at the flame wings, whereas a homogeneous distribution, similar to the experimental field, is found when the diffusive process of Ti-gas species is reduced. In addition, when considering higher diffusion for Ti-gaseous species, $TiO_2$ nanoparticles occupy a wider region compared to experiments. When reducing the diffusion process, the $TiO_2$ presence region extends over a smaller zone and a better agreement with experimental data is retrieved. The axial evolution of the conversion yield and of the volume fraction along the centerline are compared at Figs. 4a and b for the different cases. By reducing the contribution of the diffusive processes, the conversion start is delayed and a better agreement with experiments is observed. This is mainly due to the fact that $TiO_2$ presence at the flame roots close to the injection disappears when decreasing $D_k^{Ti}$ (see Fig. 3). In addition, the value of $f_v$ along the centerline increases when reducing the contribution of the diffusive processes since nanoparticles occupy a narrower region. $TiO_2$ concentration evolves similarly. As a consequence, the mean primary particle diameter, represented in Fig. 4c, is higher since its value is governed by the particle number density through condensation and coagulation processes. Overall, a better agreement with experiments is observed when the contribution of the diffusive processes of Ti-containing gaseous species is reduced. To complete the discussion on the diffusive process, a simulation without nanoparticles thermophoresis was performed with $0.1D_k^{Ti}$. Results are added to Fig. 3. No significant differences are obtained compared to the corresponding case with thermophoresis. The effect of a higher particle diffusivity, obtained by recalculating $D_p$ by assuming a constant Schmidt number of 25, is also illustrated in Fig. 3 for $0.1D_k^{Ti}$. Increasing nanoparticle diffusivity leads to a quick decay of the volume fraction along the centerline for z>40 mm. Overall, it can be concluded that the diffusive processes play an important role in the spatial localization and concentration of nanoparticles, with a direct effect on the primary particle size in non-premixed cases. It seems also that the TTIP conversion is predicted too quickly by the models available in the literature and that, by reducing the diffusion of Ti-containing species, a high concentration of Ti-species can be found downstream leading to a higher volume fraction whose maximum is localized downstream. Even if reducing diffusivities of Ti-containing gaseous species brings a better agreement with experiments, in authors' opinion, to rigorously improve the prediction accuracy, it is necessary to develop detailed kinetics mechanisms including additional Ti-species and reactions up to the Ti-precursors, which still have to be identified. By adding more intermediate reactions and species, the TTIP conversion process is expected to be slow down, consequently localizing downstream the $f_v$ peak. Such developments would require extensive database, which is not available in the literature, and are out of the scope of this work. In the following, the models parameters for the gas phase leading to a better agreement with the experimental data (model 5 and $0.1D_k^{Ti}$) will be considered to perform the sensitivity study on the aerosol process.

### *4.2. Sensitivity to aerosol process parameters*

The role of each considered aerosol process (nucleation, condensation, sintering, coagulation) and the sensitivity of their parameters are evaluated here by considering them separately. It has been observed that the volume fraction $f_v$ only slightly vary in the simulations proposed in this section, whereas the evolution of $d_p$ strongly depends on them. Thus, only results on $d_p$ are presented here.

First, the effect of the value of the collisional frequencies for nucleation $\epsilon_{nu}$ and condensation $\epsilon_{cd}$ is considered in Fig. 5 by looking at the evolution of $d_p$ along the centerline. The two processes are competing since they both depend on $(OH)_4Ti$ concentration. Nucleation will produce nuclei particles, i.e. the smallest solid particles, whereas condensation increases $d_p$ values. When increasing $\epsilon_{nu}$, the nucleation contribution is increased leading to a smaller value of $d_p$ since the available $(OH)_4Ti$ is used to generate the smallest particles. Logically, the opposite trend is then observed for condensation. When decreasing/increasing $\epsilon_{cd}$, $d_p$ decreases/increases. When neglecting condensation, a quite small $d_p$ is obtained far from the experimental values, proving that in this configuration the sintering process is not sufficient to predict $d_p$ value and that condensation (and/or surface growth) processes

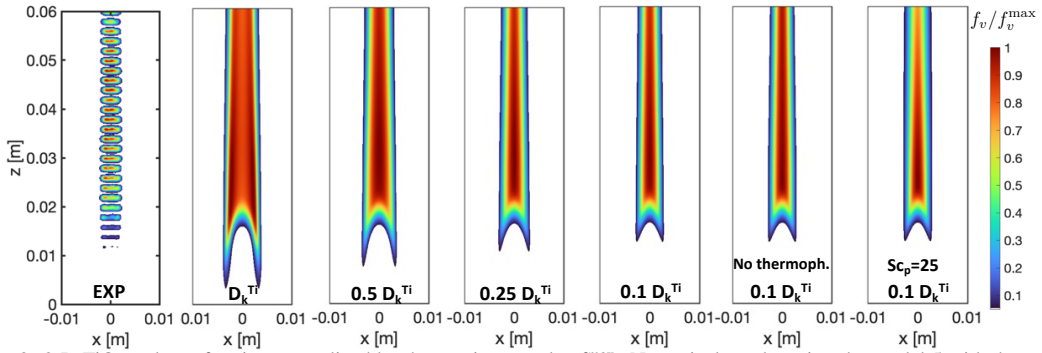


Fig. 3: 2-D $TiO_2$ volume fraction normalized by the maximum value $f_v^{max}$. Numerical results using the model 5 with decreasing diffusion coefficients are compared to the experimental signal. Results without particle thermophoresis and for particle diffusivity based on $Sc_p$=25 are also added for case $0.1 D_k^{Ti}$.

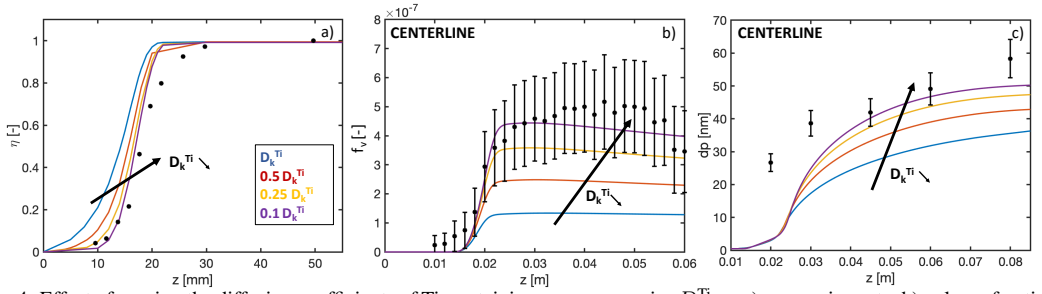


Fig. 4: Effect of varying the diffusion coefficients of Ti-containing gaseous species $D_k^{Ti}$ on a) conversion rate, b) volume fraction, and c) mean primary particle diameter along the flame centerline. Numerical results, obtained using model 5, are compared to experimental LII and SEM data (symbols).

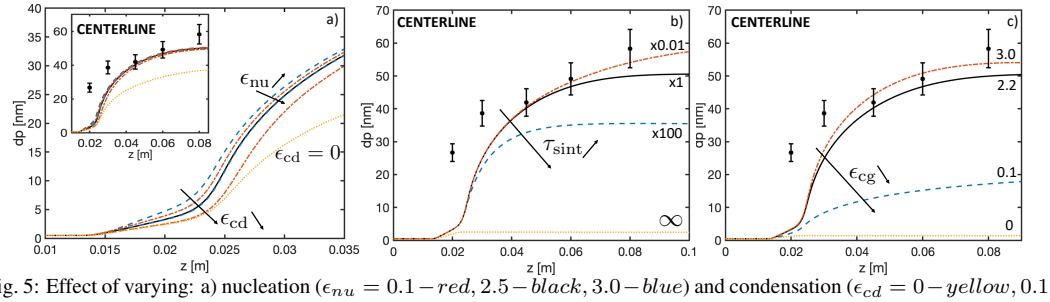


Fig. 5: Effect of varying: a) nucleation ($\epsilon_{nu} = 0.1 - red, 2.5 - black, 3.0 - blue$) and condensation ($\epsilon_{cd} = 0 - yellow, 0.1 - red, 1.3 - black, 3.0 - blue$) collisional frequencies; b) sintering time, c) coagulation collisional frequency. The numerical mean primary particle diameter is compared to SEM along the flame centerline. In a) a zoom on the early-stage formation zone is provided, whereas results over the whole flame length are illustrated into the inlay. Numerical results have been obtained using mechanism 5 and diffusion coefficients for Ti-containing gaseous species given by 0.1 $D_k^{Ti}$. Tested parameters' values for sintering and coagulation are indicated in the images.

have to be accounted for. As already deduced for premixed flames [13], the parameter's values affect $d_p$ in the early formation zone ($z$ <30 mm), whereas very similar predictions are obtained for higher heights, as visualized in the enclosed image in Fig. 5a.

Second, the role of sintering is studied in Fig. 5b, by considering reduced or enhanced values of $\tau_{sint}$. As expected, bigger $d_p$ values are obtained when increasing the sintering contribution, i.e. decreasing the sintering time. In this case, the predicted primary particle number $n_p$ is close to the unity, indicating that even by additionally enhancing the sintering process, no bigger primary particles could be obtained. The case without sintering is also reported in Fig. 5b. Small $d_p$ values are obtained indicating that sintering plays an essential role in $d_p$ growth in this configuration.

Finally, the role of coagulation on $d_p$ is discussed in Fig. 5c. Even if coagulation does not directly modify the $d_p$ size, it can indirectly affect its value by forming agglomerates and aggregates that will sinter into spherical particles of bigger diameter, espe-

cially in the early formation zone where high flame temperature and small $d_p$ values are observed. This explains why the higher $\epsilon_{cg}$, the bigger $d_p$ value is found. When coagulation is neglected, small $d_p$ values are obtained as for the case without sintering, since in practice sintering cannot contribute to $d_p$ increasing. In terms of agreement with the experimental data, a reasonable agreement is overall obtained even if too small $d_p$ values are observed at the very first stage, i.e. $z$ <25 mm, indicating the need for future modelling developments focused on the early stage of nanoparticle production.

## 5. Conclusion

In this work, numerical simulations of $TiO_2$ production in a laminar coflow $H_2$/Ar/TTIP diffusion flame have been performed by considering: 1) different submodels for the description of TTIP conversion into $Ti(OH)_4$, i.e. $TiO_2$ gaseous precursor; 2) different transport properties for Ti-containing gaseous species; 3) aerosol process parameters. The performances of the models were compared to available experimental data. 2-D LII measurements provided the $f_v$ spatial distribution and the evolution of the conversion rate $\eta$ along the centerline, which was used to evaluate the accuracy of the kinetic models for the description of TTIP conversion. Subsequently, information on mean primary particle diameter $d_p$ was used to evaluate the performances of the aerosol processes models. The parametric study on aerosol processes confirms the conclusions already obtained in premixed flames [13]. Specifically, nucleation and condensation parameters only slightly affect the results for $d_p$ downstream of the flame, but their impact is more evident in the early-stage formation zone, i.e. at small heights above the burner. On the contrary, sintering and coagulation processes more largely affect final $d_p$ values. Results for the spatial evolution along the flame of the conversion rate and of the volume fraction are not significantly affected by the parameters of the aerosol process model. On the contrary, they strongly depend on the gas phase chemistry and diffusivity of Ti-containing gaseous species. Overall, the experimental data can be qualitatively retrieved by the retained numerical strategy, even if its accuracy cannot be assessed due to the lack of an extensive experimental database. On the contrary, the early stage formation of nanoparticles (i.e. HAB$<$ 25 mm) cannot be captured with the considered models, indicating that the development of more accurate models is needed for the gaseous phase and nanoparticles. For this, additional experiments on diffusion flames are sought to define and validate the model's parameters. In future works, the polydispersity of particles should also be taken into account to evaluate the effect of the assumption of a monodisperse $TiO_2$ population on the presented conclusions.

## Declaration of competing interest

The authors declare that they have no known competing financial interests or personal relationships that could have appeared to influence the work reported in this paper.


## Acknowledgments

The support of the European Research Council (ERC) under the European Union Horizon 2020 research and innovation program (grant agreement No. 757912) is gratefully acknowledged.


## Supplementary material

Supplementary material is submitted.

## References


[1] F. Meierhofer, U. Fritsching, Synthesis of metal oxide nanoparticles in flame sprays: review on process technology, modeling and diagnostics, Energy Fuels 35 (2021) 5495–5537.

[2] S. Li, Y. Ren, P. Biswas, S. Tse, Flame aerosol synthesis of nanostructured materials and functional devices: Processing, modeling, and diagnostics, Prog. Energy Comb. Sci. 55 (2016) 1–59.

[3] V. Raman, R. Fox, Modeling of fine-particle formation in turbulent flames, Annu. Rev. Fluid Mech. 48 (1) (2016) 159–190.

[4] B. Zhao, K. Uchikawa, J. McCormick, C. Ni, J. Chen, H. Wang, Ultrafine anatase TiO2 nanoparticles produced in premixed ethylene stagnation flame at 1 atm, Proc. Combust. Inst. 30 (2005) 2569–2567.

[5] E. Tolmachoff, A. Abid, D. Phares, C. Campbell, H. Wang, Synthesis of nano-phase TiO2 crystalline films over premixed stagnation flames, Proc. Combust. Inst. 32 (2009) 1839–1845.

[6] O. Arabi–Katbi, S. Pratsinis, P. Morrison, C. Megaridis, Monitoring the flame synthesis of TiO2 particles by in-situ FTIR spectroscopy and thermophoretic sampling, Combust. Flame 124 (2019) 560–572.

[7] M. Manuputty, C. Linbderg, M. Botero, J. Akroyd, M. Kraft, Detailed characterisation of tio2 nanoaggregate morphology using TEM image analysis, J. Aerosol Sci. 133 (2019) 96–112.

[8] M. Manuputty, J. Dreyer, Y. Sheng, E. Bringley, M. Botero, J. Akroyd, M. Kraft, Polymorphism of nanocrystalline TiO2 prepared in a stagnation flame: formation of the TiO2-II phase, Chem. Sci. 10 (2019) 1342–1350.

[9] E. Bringley, M. Manuputty, C. Linbderg, G. Leon, J. Akroyd, M. Kraft, Simulations of TiO2 nanoparticles synthesised off-centreline in jet-wall stagnation flames, J. Aerosol Sci. 162 (2022) 105928.

[10] P. Buerger, D. Nurkowski, J. Akroyd, S. Mosbach, M. Kraft, First-principles thermochemistry for the thermal decomposition of titanium tetraisopropoxide, J. Phys. Chem. A 119 (2015) 8376–8387.

[11] P. Buerger, D. Nurkowski, J. Akroyd, M. Kraft, A kinetic mechanism for the thermal decomposition of titanium tetraisopropoxide, Proc. Combust. Inst. 36 (1) (2017) 1019–1027.

[12] S. Tsantilis, H. Kammler, S. Pratsinis, Population balance modeling of flame synthesis of titania particles, Chem. Eng. Science 57 (2002) 2139–2156.

[13] C. S. Lindberg, M. Y. Manuputty, J. Akroyd, M. Kraft, A two-step simulation methodology for modelling stagnation flame synthesised aggregate nanoparticles, Combust. Flame 202 (2019) 143–153.

[14] C. Lindberg, M. Manuputty, P. Buerger, J. Akroyd, M. Kraft, Numerical simulation and parametric sensitivity study of titanium dioxide particles synthesised in a stagnation flame, J. Aerosol Sci. 138 (2019) 105451.
[15] K. Wegner, S. Pratsinis, Nozzle-quenching process for controlled flame synthesis of titania nanoparticles, AIChE Journal 49 (2003) 1667–1675.
[16] K. Wegner, S. Pratsinis, Scale-up of nanoparticle synthesis in diffusion flame reactors, Chem. Eng. Sci. 58 (20) (2003) 4581–4589.
[17] K. Akurati, A. Vital, U. Klotz, B. Bommer, T. Graule, M. Winterer, Synthesis of non-aggregated titania nanoparticles in atmospheric pressure diffusion flames, Powder Technol. 165 (2006) 73–82.
[18] N. Memon, D. Anjum, S. Chung, Multiple-diffusion flame synthesis of pure anatase and carbon-coated titanium dioxide nanoparticles, Combust. Flame 160 (2013) 1848–1856.
[19] Y. Ren, K. Ran, S. Kruse, J. Mayer, H. Pitsch, Flame synthesis of carbon metal-oxide nanocomposites in a counterflow burner, Proc. Combust. Inst. 38 (1) (2021) 1269–1277.
[20] J. Yi, C. Betrancourt, N. Darabiha, B. Franzelli, Initial interpretation of laser-induced incandescence (LII) signals from flame-generated TiO2 particles: towards a quantitative characterization of the flame synthesis processes, App. Energy Combust. Sci. 15 (2023) 100190.
[21] P. B. Kuhn, B. Ma, B. C. Connelly, M. D. Smooke, M. B. Long, Soot and thin-filament pyrometry using a color digital camera, Proc. Combust. Inst. 33 (1) (2011) 743 – 750.
[22] M. Smooke, M. Long, B. Connelly, M. Colket, R. Hall, Soot formation in laminar diffusion flames, Combust. Flame 143 (4) (2005) 613–628.
[23] N. Kempema, M. Long, Combined optical and TEM investigations for a detailed characterization of soot aggregate properties in a laminar coflow diffusion flame, Combust. Flame 164 (2016) 373–385.
[24] J. Yi, C. Betrancourt, N. Darabiha, B. Franzelli, Characterization of laser-induced emission of high-purity TiO2 nanoparticles: feasibility of laser-induced incandescence, App. Physics B 129 (2023) 1–19.
[25] Z. Li, H. Wang, Thermophoretic force and velocity of nanoparticles in the free molecule regime, Phys. Rev. E 70 (2004).
[26] C. Betrancourt, F. Liu, P. Desgroux, X. Mercier, A. Faccinetto, M. Salamanca, L. Ruwe, K. Kohse-Hoinghaus, D. Emmrich, A. Beyer, A. Golzhauser, T. Tritscher, Investigation of the size of the incandescent incipient soot particles in premixed sooting and nucleation flames of n-butane using LII, HIM, and 1 nm-SMPS, Aerosol Sci. Tech. 51 (8) (2017) 916–935.
[27] A. Cuoci, A. Frassoldati, T. Faravelli, E. Ranzi, Numerical modeling of laminar flames with detailed kinetics based on the operator-splitting method, Energy and Fuels 27 (2013) 7730–7753.
[28] E. Ranzi, A. Frassoldati, A. Stagni, M. Pelucchi, A. Cuoci, T. Faravelli, Reduced kinetic schemes of complex reaction systems: Fossil and biomass-derived transportation fuels, Int. J. Chem. Kinetics 46 (2014) 512–542.
[29] K. Okuyama, R. Ushio, Y. Kousaka, R. Flagan, J. Seinfeld, Particle generation in a chemical vapor deposition process with seed particles, AiChE J. 36 (1990) 409–419.
[30] T. Seto, M. Shimada, K. Okuyama, Evaluation of sintering of nanometer-sized titania using aerosol method, Aerosol Sci. Tech. 23 (1995) 183–200.
[31] J. Wei, A. Ostadhossein, S. Li, M. Ihme, Kinetics for the hydrolysis of Ti(OC3H7)4: A molecular dynamics simulation study, Proc. Combust. Inst. 38 (1) (2021) 1433–1440.
[32] A. Shmakov, O. Korobeinichev, D. Knyazkov, A. Paletsky, R. Maksyutov, I. Gerasimov, T. Bolshova, V. Kiselev, N. Gritsan, Combustion chemistry of ti(oc3h7)4 in premixed flat burner-stabilized H2/O2/Ar flame at 1 atm, Proc. Combust. Inst. 34 (2013) 1143–1149.
[33] J.-M. Orlac'h, N. Darabiha, V. Giovangigli, B. Franzelli, Importance of mass and enthalpy conservation in the modeling of titania nanoparticles flame synthesis, Combust. Theory and Modelling 15 (2021) 389–412.
[34] B. Franzelli, A. Vié, N. Darabiha, A three-equation model for the prediction of soot emissions in LES of gas turbines, Proc. Combust. Inst. 37 (2019) 1344 – 1363.
[35] G. Kelesidis, M. Reza Kholghy, A Monodisperse Population Balance Model for Nanoparticle Agglomeration in the Transition Regime, Materials 14 (2021) 3882.
[36] A. Abdelsamie, F. Kruis, H. Wiggers, D. Thevenin, Nanoparticle Formation and Behavior in Turbulent Spray Flames Investigated by DNS, Flow Turbulence and Combustion 105 (2020) 497 – 516.
[37] A. Rittler, L. Deng, I. Wlokas, A.M. Kempf, Large eddy simulations of nanoparticle synthesis from flame spray pyrolysis, Proc. Combust. Inst. 36 (2020) 1077 – 1086.
[38] M. Mueller, G. Blanquart, H. Pitsch, A joint volume-surface model of soot aggregation with the method of moments, Proc. Combust. Inst. 32 (1) (2009) 785 – 792.